Magnetic Resonance Imaging

DOI: 10.1002/ange.201409365

Activatable ^{19}F MRI Nanoparticle Probes for the Detection of Reducing Environments**

*Tatsuya Nakamura, Hisashi Matsushita, Fuminori Sugihara, Yoshichika Yoshioka, Shin Mizukami, and Kazuya Kikuchi**

Abstract: *^{19}F magnetic resonance imaging (MRI) probes that can detect biological phenomena such as cell dynamics, ion concentrations, and enzymatic activity have attracted significant attention. Although perfluorocarbon (PFC) encapsulated nanoparticles are of interest in molecular imaging owing to their high sensitivity, activatable PFC nanoparticles have not been developed. In this study, we showed for the first time that the paramagnetic relaxation enhancement (PRE) effect can efficiently decrease the ^{19}F NMR/MRI signals of PFCs in silica nanoparticles. On the basis of the PRE effect, we developed a reduction-responsive PFC-encapsulated nanoparticle probe, FLAME-SS-Gd^{3+} (FSG). This is the first example of an activatable PFC-encapsulated nanoparticle that can be used for in vivo imaging. Calculations revealed that the ratio of fluorine atoms to Gd^{3+} complexes per nanoparticle was more than approximately 5.0×10^2, resulting in the high signal augmentation.*

Molecular imaging techniques have emerged as promising tools for monitoring the dynamics, localization, and concentrations of biomolecules in living systems.[1] Recently, magnetic resonance imaging (MRI) has received considerable attention because of its prominent properties such as deep tissue imaging and high spatial resolution.[2] In particular, ^{19}F MRI has an advantage over ^{1}H MRI owing to the lack of endogenous background signals. Though several activatable ^{19}F MRI probes capable of detecting enzymatic activity and pH have been reported,[3,4] there are only a few examples of in vivo applications owing to the low sensitivity of such probes. In the last decade, perfluorocarbon (PFC) encapsulated nanoemulsions have attracted significant attention as highly sensitive ^{19}F MRI contrast agents (always ON-type probes).[5] We developed a highly sensitive ^{19}F MRI contrast agent comprised of a perfluoro[15]crown-5-ether (PFCE) core and a silica shell, termed FLAME.[6] FLAME has superior properties such as high sensitivity, stability in both aqueous and organic solutions, facile surface modifications, and biocompatibility. Through adequate surface modifications of FLAME, various applications such as protein labeling, cell labeling, and tumor targeting were achieved.[6] However, to the best of our knowledge, activatable PFC-encapsulated nanoparticles (switching OFF/ON-type probes) have not been reported. Thus, activatable PFC nanoparticles are highly desirable to realize various applications.

The potential for facile surface modifications on FLAME motivated us to introduce the paramagnetic relaxation enhancement (PRE) effect of Ln^{3+} complexes to create an OFF/ON switching ability. We exploited the PRE effect for T_2 modulation in small-molecule ^{19}F MRI probes.[4] The PRE effect is effective over short distances because of its r^{-6} dependency, where r is the distance between nuclei observable by NMR spectroscopy and a paramagnetic center (up to 35 Å for Mn^{2+}).[7,8] Because most PFCE compounds in FLAME are more than 50 Å away from the surface-modified Ln^{3+} complexes because of the thickness of the silica shell (Figure S1a), it was assumed that the PRE effect might not sufficiently attenuate the ^{19}F NMR/MRI signals of FLAME.

We first confirmed whether the PRE of the Gd^{3+} complexes on the FLAME surface was effective. Gd^{3+} diethylenetriaminepentaacetate (DTPA) complexes were attached to FLAME to yield FLAME-DTPA-Gd (Figure 1, Scheme S1). The ^{19}F NMR spectrum of FLAME-DTPA without Gd^{3+} exhibited a sharp, single peak ($T_2 = 420$ ms). Meanwhile, that of FLAME-DTPA-Gd showed a broad peak ($T_2 =$ 40 ms; Figure 2a, Table S1). Although the ^{19}F MRI signals of FLAME-DTPA were observed because of the long T_2, that of FLAME-DTPA-Gd was efficiently quenched (Figure 2b). These results indicated that the ^{19}F NMR/MRI signals of PFCE in FLAME were affected by the PRE from the surface-modified Gd^{3+} complexes. Therefore, we expected that activatable ^{19}F MRI probes with high ^{19}F MRI signal enhancement would be achieved by introducing a cleavable linker between FLAME and the surface-modified Gd^{3+} complexes.

This result was explained by the molecular mobility on the NMR/MRI measurement time scale. Iwahara and Clore reported that the PRE effect was efficient in spite of the long average distance, when nuclei observable by NMR spectroscopy can occasionally enter the effective range of the PRE effect.[8] The long T_2 indicates that the PFCE in FLAME

[*] T. Nakamura, Dr. H. Matsushita, Dr. S. Mizukami, Prof. K. Kikuchi
Graduate School of Engineering, Osaka University
Yamadaoka 2-1, Suita, Osaka 565-0871 (Japan)
E-mail: kkikuchi@mls.eng.osaka-u.ac.jp
Dr. F. Sugihara, Prof. Y. Yoshioka, Dr. S. Mizukami, Prof. K. Kikuchi
Immunology Frontier Research Center, Osaka University
Yamadaoka 3-1, Suita, Osaka 565-0871 (Japan)

[**] This research was supported by the Ministry of Education, Culture, Sports, Science, and Technology (Japan) (grant numbers 24685028, 25620133, 25220207, and 26102529), and by CREST from JST. The authors acknowledge the Asahi Glass Foundation and the Magnetic Health Science Foundation. The authors thank Dr. Takao Sakata (Osaka University) for his support with TEM measurements. Some of the experiments were carried out at the Research Center for Ultra-High Voltage Electron Microscopy, Osaka University. MRI = magnetic resonance imaging.

Supporting information for this article is available on the WWW under http://dx.doi.org/10.1002/anie.201409365.

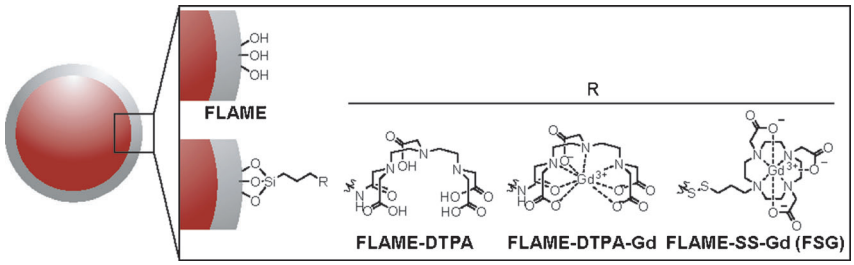

Figure 1. Chemical structure of prepared nanoparticles.

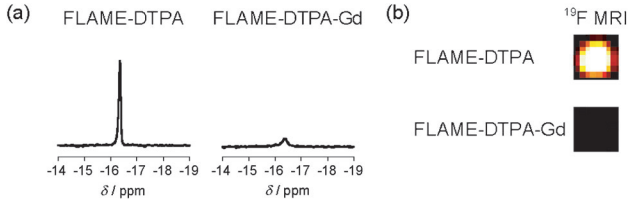

Figure 2. a) ^{19}F NMR spectra and b) ^{19}F MRI phantom images of FLAME-DTPA and FLAME-DTPA-Gd. For ^{19}F NMR, $C_{PFCE} = 0.6$ mM, and the accumulation time was 1 min 22 s. For ^{19}F MRI (rapid acquisition with the refocused echoes (RARE) method): T_R was 3000 ms. $T_{E,eff}$ was 12 ms. The number of excitations (NEX) was 64. The acquisition time was 12 min 48 s.

maintains high molecular mobility even in the nanoparticle structure.[6] Although the PFCE at the center of the FLAME core is about 250 Å away from the surface Gd^{3+} complexes (where PRE is not efficient), the fluorine compounds can access the inner shell of FLAME on the measurement time scale. Near the inner shell, although the contribution of one Gd^{3+} complex to the PRE effect is small, the PRE effect from multiple surface Gd^{3+} complexes is combined, and thus the T_2 of PFCE is efficiently decreased. Although Grüll and co-workers observed the PRE of PFCE in Gd^{3+}-modified nanoemulsions, where the distance between the Gd^{3+} complexes and the fluorine core was less than 22 Å,[9] we confirmed that the PRE was effective as such distance for the first time.

Next, we designed activatable FLAMEs, FLAME-SS-Gd^{3+} (FSG), to image reducing environments. Redox reactions play crucial roles in biological processes, and abnormal redox reactions are implicated in various conditions including liver damage, and human immunodeficiency virus.[10] Gd^{3+} complexes were attached to the FLAME surface by disulfide linkers to reduce the T_2 of the fluorine compounds by the PRE effect, which attenuates the ^{19}F NMR/MRI signals (Figure 3). When the disulfide of FSG was reduced, the Gd^{3+} complexes were cleaved from the FLAME surface. Then, the T_2 of the encapsulated PFCE would be elongated and the ^{19}F NMR/MRI signal intensity would increase.

To optimize the amount of surface Gd^{3+} complexes, three types of FSGs with different concentrations of Gd^{3+} were prepared (Scheme S2). The average diameter of FLAME was 53.4 nm with a 5 nm-thick silica shell, as measured by transmission electron microscopy (Figure S1). The amount of fluorine atoms and Gd^{3+} ions per nanoparticle were calculated from ^{19}F NMR spectroscopy and inductively coupled plasma atomic emission spectrometry (Table 1; details

Table 1: Properties of FLAME and FSGs.

Materials	n_{19F}[a]	n_{Gd}[a]	n_{19F}/n_{Gd}[a]	$T_{2,TCEP(-)}$ [ms]	$T_{2,TCEP(+)}$ [ms]
FLAME	1.7×10^6	0	–	420	–[b]
FSG1	1.7×10^6	9.1×10^2	1.8×10^3	120	383
FSG2	1.7×10^6	2.1×10^3	7.7×10^2	66	365
FSG3	1.7×10^6	3.1×10^3	5.3×10^2	27	371

[a] These values were predicted assuming that FSG has a single size of 53.4 nm (diameter). [b] Not measured. n_{19F}: the number of ^{19}F atoms in one nanoparticle. n_{Gd}: the number of Gd^{3+} atoms in one nanoparticle.

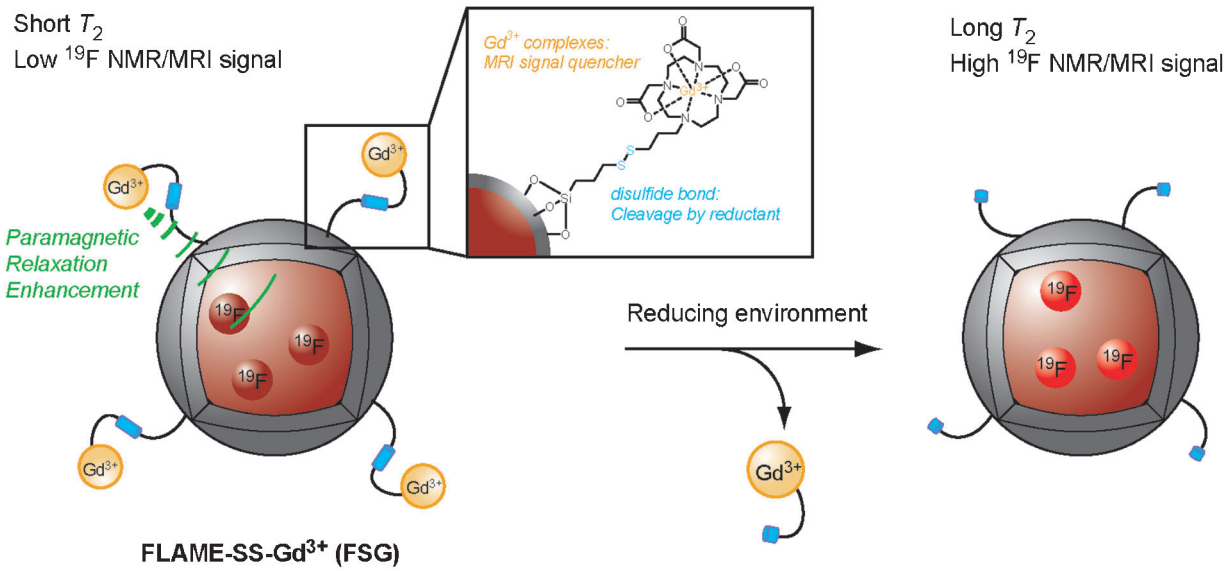

Figure 3. Design of activatable FLAME, FLAME-SS-Gd^{3+} (FSG).

regarding the calculations are given in the Supporting Information). The ratio values of n_{19F} to n_{Gd} on a single nanoparticle were estimated to be 1.8×10^3, 7.7×10^2, and 5.3×10^2 for FSG1-3, respectively.

The ^{19}F NMR peaks of FSGs without a reducing agent were shorter and broader than that of FLAME according to the Gd^{3+} concentration-dependent PRE effect (Figure 4a). The ^{19}F NMR signal-to-noise ratio (SNR) indicated that FSG3 were most quenched (Figure 4b). The T_2 of FSGs decreased with increasing amounts of Gd^{3+} (Table 1). As such, the PRE effect was efficient in all FSGs.

Next, ^{19}F NMR spectra and T_2 of FSGs were measured after treatment with a reducing agent, tris(2-carboxyethyl)-phosphine (TCEP; Figure 4 and Figure S3). Addition of TCEP made the ^{19}F NMR peaks of all FSGs sharper and taller as compared to those before the addition. The T_2 values of FSG1-3 were significantly increased upon addition of TCEP within 2 h (Table S3), and were comparable to that of FLAME (Table 1). All Gd^{3+} complexes were cleaved upon addition of more than 2 mM TCEP (Figure 4b and Figure S4). The highest ^{19}F NMR SNR values for all FSGs were obtained with 2 mM TCEP. The signal enhancement factors in response to the reductant were 3.1, 9.7, and 12.7 for FSG1-3, respectively. Thus, FSG3 was the most sensitive ^{19}F NMR probe in the detection of the reducing environment.

The ^{19}F NMR signals of the FSGs increased upon addition of other reducing agents such as glutathione, cysteine, and dithiothreitol (Figure S5). In particular, addition of glutathione induced the greatest ^{19}F NMR signal enhancement. Glutathione levels in breast and colon cancer-ridden tissues are higher than those in normal tissues.[11] Since FSGs were stable under physiological conditions (Table S3, Figure S6), FSGs can be potentially useful for the selective detection of high glutathione concentrations. Although there are some concerns about the stability of reduction-triggered nanoparticles in normal tissues, rational optimization of the disulfide linkage will lead to practical in vivo applications.

Finally, ^{19}F MR phantom images of FSGs solutions with or without TCEP were obtained by varying $T_{E,eff}$. In general, the MRI signal of the long T_2 component is well-observed at both short and long $T_{E,eff}$. In contrast, the MRI signal of samples with moderately short T_2 is only visible at short $T_{E,eff}$, and that of the extremely short T_2 component is not observed even at short $T_{E,eff}$. As expected from the ^{19}F NMR results, almost no ^{19}F MRI signals of FSG2 and FSG3 were detected without TCEP at any $T_{E,eff}$ because of the strong PRE effect (Figure 5a and b). In contrast, the ^{19}F MRI signals of FSG1 were observed at $T_{E,eff} \leq 84$ ms because of the moderately short T_2. However, the measurement of FSG1 without TCEP at $T_{E,eff} \geq 108$ ms extinguished the undesired ^{19}F MRI signals. Reductive reactions induced a noticeable ^{19}F MRI signal enhancement in FSG1-3 at any $T_{E,eff}$ (filled circles). At $T_{E,eff} = 12$ ms, approximately 60- and 40-fold increases were observed in FSG2 and FSG3, respectively. Although the signal enhancement of FSG1 was only two-fold at $T_{E,eff} = 12$ ms, a 50-fold increase was observed at $T_{E,eff} = 108$ ms. These results indicated that FSG2 was the most effective probe for detecting reducing environments. One of the advantages of FSGs is the high sensitivity, because the ^{19}F NMR/MRI signals of 1.7×10^6 fluorine atoms in the core were decreased by approxiomately 1.0×10^3 Gd^{3+} complexes on the FLAME surface. The ratios of fluorine atoms to Gd^{3+} complexes (Table 1) are the highest among known PRE-based probes, of which the ratios were single digits.[4,12] This high ratio led to the high signal amplification.

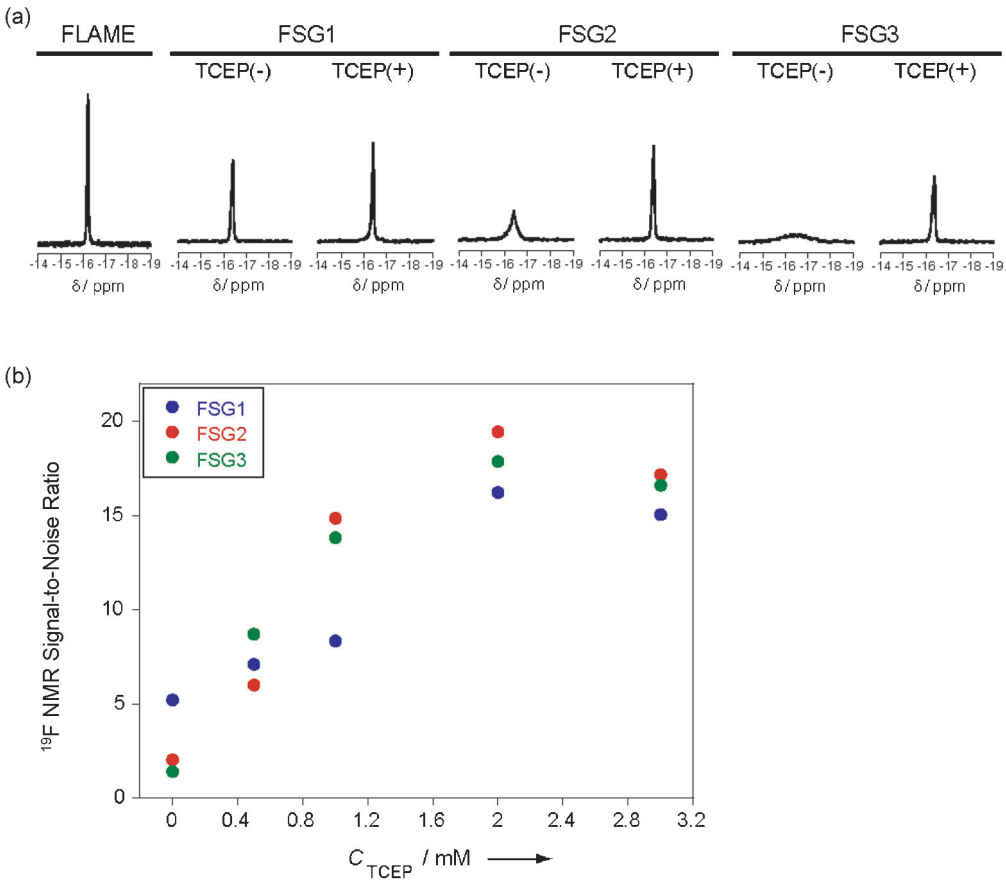

Figure 4. a) ^{19}F NMR spectra of FSGs incubated with or without TCEP. C_{PFCE}: 0.6 mM, C_{TCEP}: 1.0 mM, incubation time: 4 h, accumulation time: 10 min 55 s. b) ^{19}F NMR signal-to-noise ratio of FSGs in the presence of TCEP (blue: FSG1, red: FSG2, green: FSG3). C_{PFCE}: 0.15 mM.

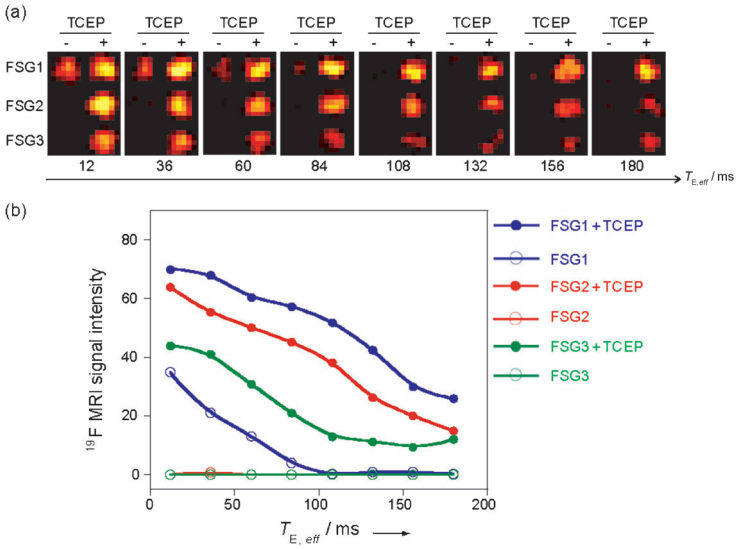

Figure 5. ^{19}F MRI signal enhancement of FSGs by TCEP. a) ^{19}F MRI phantom images of FSG1-3 with or without TCEP. b) Plot of ^{19}F MRI signal intensity of FSG1-3 at different $T_{E,eff}$ with (filled circles) or without (open circles) TCEP. ^{19}F MRI RARE method: T_R was 3000 ms. The number of excitations (NEX) was 64. The acquisition time was 25 min 36 s.

In conclusion, we showed for the first time that the PRE effect of surface Gd^{3+} complexes was effective for fluorine compounds in nanoparticles over 50 Å. On the basis of this finding, we developed novel ^{19}F MRI probes, FSGs, which could visualize reducing environments. FSGs are the first example of activatable ^{19}F MRI nanoparticle probes with high signal amplification, because the FSGs had exceedingly high ratios of fluorine atoms to Gd^{3+} complexes. Since FLAME has superior properties such as stability, high sensitivity, and biocompatibility,[6] activatable FLAMEs are quite promising for in vivo applications. In particular, activatable FLAMEs should be useful for visualizing the activities of dilute biomolecules such as enzymes, by introducing substrate–peptide sequences instead of disulfide linkers. We believe that PRE-based activatable FLAMEs will facilitate a change in in vivo imaging probes.

Received: September 22, 2014
Revised: October 24, 2014
Published online: November 24, 2014

Keywords: activatable probes · fluorine · imaging agents · magnetic resonance imaging · nanoparticles

[1] a) R. Weissleder, M. J. Pittet, *Nature* **2008**, *452*, 580–589; b) R. H. Newman, M. D. Fosbrink, J. Zhang, *Chem. Rev.* **2011**, *111*, 3614–3666.
[2] a) A. Y. Louie, M. M. Hüber, E. T. Ahrens, U. Rothbächer, R. Moats, R. E. Jacobs, S. E. Fraser, T. J. Meade, *Nat. Biotechnol.* **2000**, *18*, 321–325; b) J.-X. Yu, R. R. Hallac, S. Chiguru, R. P. Mason, *Prog. Nucl. Magn. Reson. Spectrosc.* **2013**, *70*, 25–49; c) S. J. Ratnakar, S. Viswana-than, Z. Kovacs, A. K. Jindal, K. N. Green, A. D. Sherry, *J. Am. Chem. Soc.* **2012**, *134*, 5798–5800.
[3] a) J.-X. Yu, V. D. Kodibagkar, R. R. Hallac, L. Liu, R. P. Mason, *Bioconjugate Chem.* **2012**, *23*, 596–603; b) K. Yamaguchi, R. Ueki, H. Nonaka, F. Sugihara, T. Matsuda, S. Sando, *J. Am. Chem. Soc.* **2011**, *133*, 14208–14211; c) X. Huang, G. Huang, S. Zhang, K. Sagiyama, O. Togao, X. Ma, Y. Wang, Y. Li, T. C. Soesbe, B. D. Sumer, M. Takahashi, A. D. Sherry, J. Gao, *Angew. Chem. Int. Ed.* **2013**, *52*, 8074–8078; *Angew. Chem.* **2013**, *125*, 8232–8236; d) K. Tanaka, N. Kitamura, K. Naka, Y. Chujo, *Chem. Commun.* **2008**, 6176–6178.
[4] a) S. Mizukami, R. Takikawa, F. Sugihara, Y. Hori, H. Tochio, M. Wälchli, M. Shirakawa, K. Kikuchi, *J. Am. Chem. Soc.* **2008**, *130*, 794–795; b) S. Mizukami, H. Matsushita, R. Takikawa, F. Sugihara, M. Shirakawa, K. Kikuchi, *Chem. Sci.* **2011**, *2*, 1151–1155.
[5] E. T. Ahrens, R. Flores, H. Xu, P. A. Morel, *Nat. Biotechnol.* **2005**, *23*, 983–987.
[6] H. Matsushita, S. Mizukami, F. Sugihara, Y. Nakanishi, Y. Yoshioka, K. Kikuchi, *Angew. Chem. Int. Ed.* **2014**, *53*, 1008–1011; *Angew. Chem.* **2014**, *126*, 1026–1029.
[7] G. M. Clore, J. Iwahara, *Chem. Rev.* **2009**, *109*, 4108–4139.
[8] J. Iwahara, G. M. Clore, *Nature* **2006**, *440*, 1227–1230.
[9] A. De Vries, R. Moonen, M. Yildirim, S. Langereis, R. Lamerichs, J. A. Pikkemaat, S. Baroni, E. Terreno, K. Nicolay, G. J. Strijkers, H. Grüll, *Contrast Media Mol. Imaging* **2014**, *9*, 83–91.
[10] a) D. M. Townsend, K. D. Tew, H. Tapiero, *Biomed. Pharmacother.* **2003**, *57*, 145–155; b) L. A. Herzenberg, S. C. De Rosa, J. G. Dubs, M. Roederer, M. T. Anderson, S. W. Ela, S. C. Deresinski, *Proc. Natl. Acad. Sci. USA* **1997**, *94*, 1967–1972.
[11] a) R. P. Perry, J. Mazetta, M. Levin, S. C. Barranco, *Cancer* **1993**, *72*, 783–787; b) S. C. Barranco, R. R. Perry, M. E. Durm, M. Quraishi, A. L. Werner, S. G. Gregorcyk, P. Kolm, *Dis. Colon Rectum* **2000**, *43*, 1133–1140; c) M. J. Allalunuis-Turner, F. Y. F. Lee, D. W. Siemann, *Cancer Res.* **1988**, *48*, 3657–3660.
[12] a) E. De Luca, P. Harvey, K. H. Chalmers, A. Mishra, P. K. Senanayake, J. I. Wilson, M. Botta, M. Fekete, A. M. Blamire, D. Parker, *J. Biol. Inorg. Chem.* **2014**, *19*, 215–227; b) A. Keliris, I. Mamedov, G. E. Hagberg, N. K. Logothetis, K. Scheffler, J. Engelmann, *Contrast Media Mol. Imaging* **2012**, *7*, 478–483.